Numerical and experimental analysis of microwave micro-plasmas in air

P. Coche[1], L.L. Alves[1], V. Guerra[1], K. Gadonna[2], G.D. Stancu[3], O. Leroy[2], and T. Minea[2]

[1]*Instituto de Plasmas e Fusão Nuclear, Instituto Superior Técnico, Universidade de Lisboa, Lisboa, Portugal*
[2]*LPGP, UMR 8578: CNRS-Université Paris-Sud, 91405 Orsay, France*
[3]*CentraleSupélec, EM2C, CNRS UPR 288, Grande Voie des Vignes, 92290 Châtenay-Malabry, France*

Micro-plasmas have been generated in dry air using microwaves (2.45 GHz excitation frequency and ~100 W coupled power), within capillaries (< 1 mm inner radius) at low pressure (300 Pa), and characterized using both self-consistent modelling and experimental measurements. We report high dissociation degree of molecular oxygen (~70%), high concentration of $O_2(a)$ (10^{14} cm^{-3}) and of NO (10^{14} cm^{-3}), and low ozone production (< 1%).

1. Introduction

Plasmas generated in capillaries (radius less than a millimetre) have recently aroused important research efforts due to their interesting properties for applications such as synthesis of nanostructures [1,2], photonics [3], sterilization [4] and micro-propulsion [5]. In this work, we focus on microwave-sustained micro-plasmas in dry air (N_2 80% - O_2 20%), confined within a small radius capillary (R=345 μm) at low pressure (p=300 Pa).

The low-pressure microwave micro-plasma is characterized using both self-consistent modelling and experimental measurements. Modelling involves tackling new challenges, as compared to studies developed for discharges with tube radii of the order of the cm [6,7]. A major question lies on the description of the radial transport of charged particles in a weakly electronegative plasma, in a situation where the classical ambipolar theory fails. Measurements are particularly difficult also, due to the reduced discharge volume. Here, non-intrusive optical emission spectroscopy (OES) diagnostics are chosen [8], to obtain the relative and the absolute intensities of relevant radiative transitions.

2. Theoretical formulation

The simulations are performed using the LoKI (LisbOn KInetics) numerical code, which keeps the same algorithmic structure and calculation blocks used in previous publications [6,7]. The 0D (volume averaged) model couples the homogeneous two-term electron Boltzmann equation (EBE) (for the gas mixture considered, including first and second kind collisions) to a system of rate balance equations for the dominant neutral and charged species. All cross sections used are or will be available in the near future, at the IST-LISBON database of LXCat [9]. The rate balance equations concern the following main neutral / charged species: vibrationally excited states of ground-state molecular nitrogen N_2(X, v=0-59); electronically excited states N_2(A, B, C, a, a', w); ground-state and electronically excited molecules O_2(X, a, b), NO(X, A, B), NO_2(X, A), O_3 and O_3*; ground-state and electronically excited atoms N(^{4}S, ^{2}D, ^{2}P) and O(^{3}P, ^{1}D); positive ions N^+, N_2^+(X, B), N_3^+, N_4^+, O^+, O_2^+ and NO^+; negative ion O^-.

Working at low pressure (< 1000 Pa) and low radius (< 500 μm) results in a high reduced electric field and a non-classical ambipolar transport for charged particles. Two achievements were ensured to address these issues: the extension of the kinetic-energy grid up to 1000 eV, to describe the effect of the high-energy mechanisms impacting significantly on the tail of the electron energy distribution function, and the development of a transport theory valid for pR conditions beyond the limit of the classical ambipolar theory.

A careful review of existing transport theories for charged particles was made by Phelps [10], defining the transition from low (collisionless) to high pressures, and from independent motion to ambipolar plasma. The former transition is characterized by the ratio Λ/λ_i – where $\Lambda=R/2.405$ is the diffusion length for infinite cylindrical geometry and λ_i is the ion mean-free-path – whereas the latter one is connected to the ratio Λ/λ_{De} – where λ_{De} is the Debye length. Assuming typical operating conditions, electron density $n_e \simeq 4\times10^{12}$ cm^{-3}, gas temperature $T_g \simeq 1000$ K and electron temperature $T_e \simeq 10$ eV, we have $\Lambda/\lambda_{De} \sim 15$, corresponding to a dense plasma ("ambipolar regime"), and $\Lambda/\lambda_i \sim 0.25$, corresponding to low-pressure.

A transport theory embedding the transition from low to high pressures in dense plasmas was derived by Self and Ewald [11] and reformulated by Ferreira and Ricard [12], for a single type of positive ions. Since in N_2-O_2 mixtures there are several important ions, we have generalized the theory of Self and Ewald to account for several positive ions (listed in

the beginning of this section) and, at low pressures, for one (low-density) negative ion species. As in [11], the assumptions of quasi-neutrality and flux conservation are imposed. In addition, negative ions are assumed to be confined in the core of the plasma, with negligible drift velocity at low pressure [13,14]. Under these hypotheses, and by further assuming a low density for O^-, it is possible to recover a system of equations formally identical to the one of [11], whose numerical solution can be avoided using the results of [12] as an abacus.

Figure 1 shows the self-consistent calculated values of the reduced electric field, E/N, and of the electron kinetic temperature, T_e, as a function of R, using three different descriptions of the charged particle transport: the current formulation for several positive ions and one negative ion; the current formulation neglecting the effect of negative ions; and the classical ambipolar diffusion.

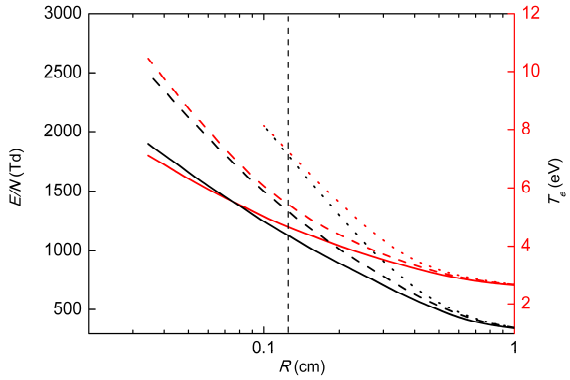

Figure 1. Reduced electric field (left axis, black) and electron temperature (right axis, red) for p=300 Pa, T_g=1100 K and n_e=3.84x10^{12} cm^{-3}, as a function of the tube radius, calculated using: the present theory (full line); the present theory neglecting the effect of negative ions (dashed line); the classical ambipolar theory (dotted line). The short-dashed vertical line limits the R-region of low pressure conditions.

Our model calculations in the presence of O^- ions should be restricted to low-pressures only ($\Lambda/\lambda_i \leq 1$, corresponding to $R \leq 0.12$ cm). Hence, the calculations performed considering the presence of both positive and negative ions should be limited to the region on the left of the short-dashed vertical line. However, as R increases the influence of negative ions becomes negligible and the present formulation can still be used, albeit with caution. Moreover, the different transport descriptions considered yield similar results at high R, confirming the classical ambipolar diffusion limit at $\Lambda/\lambda_i \gg 1$.

3. Experimental setup and diagnostics

The experimental setup, operating at LPGP, is represented in figure 2.

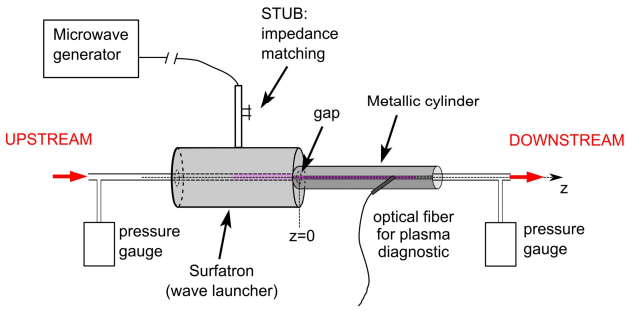

Figure 2. Schematic representation of the experimental setup.

The capillary is inserted into a wave launcher (surfatron) especially adapted to the system geometrical dimensions, ensuring a maximum electric field at the surfatron gap. Dry air is introduced from the left end of the capillary at negligible gas flow. Thus, the pressure is constant along the plasma column, being monitored up- and downstream by two pressures gauges. The system generates stable plasmas with ~3 cm length (the addition of small traces of a noble gas increases this length considerably).

Axially-resolved OES diagnostics are used to determine the absolute and relative intensities of several radiative transitions, the electron density and the gas temperature. The absolute calibration of the spectra was performed at EM2C, using a standard tungsten lamp for which the spectral radiance (in W cm^{-2} sr^{-1} nm^{-1}) is known. The same detection system (including the spectrometer and the optical collection system) is employed for recording both the discharge and the lamp spectra, the former being converted in radiance units by using the sensitivity response function. The absolute density of a particular electronic excited state is obtained by comparing measured and Specair-simulated [15] spectra.

The electron density is measured from the contribution of the Stark effect to the broadening of the Balmer line H_β. Other contributions to this broadening, such as instrumental and Van der Waals, are removed from the measured line after deconvolution. Doppler broadening is also accounted for, its contribution being much larger than Stark's for low values of n_e. This limits the actual measurement of the electron density, providing information on its upper limit only, $n_e <$ 1.4x10^{13} cm^{-3}. Thus the electron density is estimated here from a semi-empirical analysis of the power

coupled to the plasma, which provides values in agreement with the experimental upper limit.

The procedure to obtain the gas temperature is based on the measurement of the band radiative emission with the second positive system (SPS) N2(C→B), and on the simulation of the corresponding synthetic spectrum, using Specair software [15]. Figure 3 presents a typical ro-vibrational spectrum of the SPS (Δv=-2 sequence, 360-380 nm), measured using OES diagnostics and fitted using Specair simulations to determine the rotational and the vibrational temperatures T_{rot} and $T_{vib,}$ respectively. The gas temperature is identified with the rotational temperature $T_{rot,}$ by assuming that the distribution of N_2(C) reflects that of ground-state N_2(X) molecules, corrected by the appropriate Franck-Condon factors.

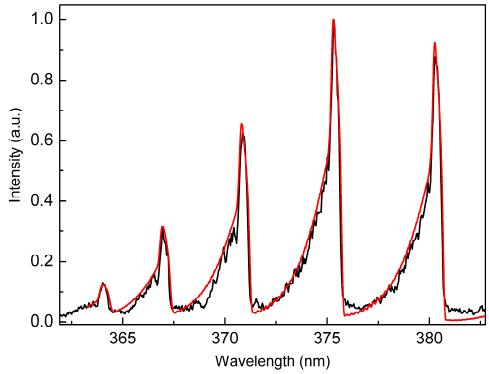

Figure 3. Comparison between SPS N2(C→B) ro-vibrational spectra, measured (black curve) and calculated with Specair (red), at 82 W coupled power, yielding T_{rot}≈1100 K and T_{vib}≈10000 K.

4. Results and discussion

Figure 4 presents the electron density and the gas temperature (obtained as described in section 3), as a function of the axial position in the plasma column, obtained for 129 W coupled power resulting in a plasma column of 1.7 cm. Due to geometrical constraints of the surfatron, the profiles starts at 0.8 cm, corresponding to the closest axial position near the surfatron gap accessible by the line-of-sight of OES diagnostics. The values of n_e and T_g presented in figure 4 (for the latter we adopt the numerical fit plotted in this figure) are used as input parameters to the model (together with p and R), to simulate the plasma for each axial position.

For the same condition as before, figure 5 compares measurements and simulations of the relative intensity with the atomic transition of triplets N($3p^4S$)→N($3s^4P$) and O($3p^5P$)→O($3s^5S$), as a function of the axial position in the plasma column. Results show that the model predicts the correct trend for the axial evolution of these line transitions.

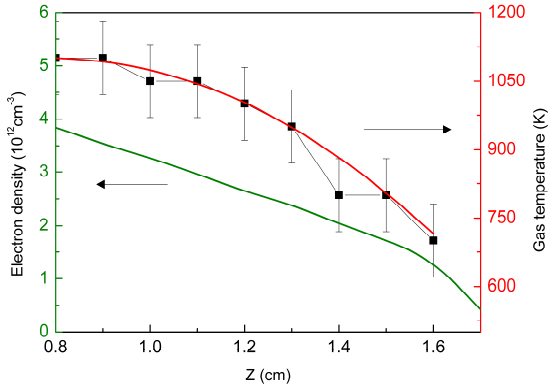

Figure 4. Axial profiles of the measured gas temperature (points and red curve as fit; right axis) and the (semi-empirically) calculated electron density (green; left), obtained at 129 W coupled power for a plasma column of 1.7 cm length.

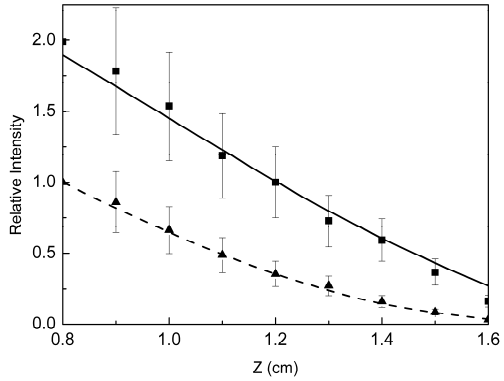

Figure 5. Axial profiles of the relative intensities with atomic line transitions, obtained at 129 W coupled power for: N($3p^4S$)→N($3s^4P$) at 744.23 nm, measured (squares) and simulated (full line); O($3p^5P$)→O($3s^5S$) at 777.19 nm, measured (triangles) and simulated (dashed line).

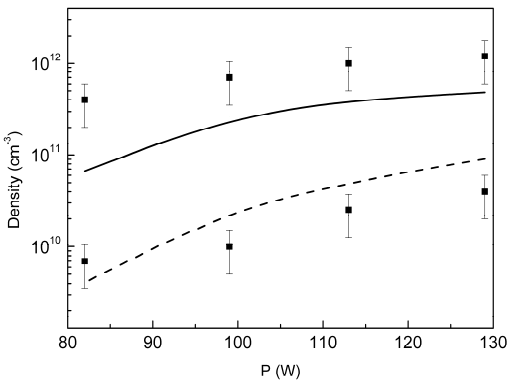

Figure 6. Calculations (curves) and measurements (points) of the absolute densities of N_2(C) (solid line) and N_2^+(B) (dashed), as a function of the power coupled to the plasma.

Figure 6 presents, as a function of the power coupled to the plasma, measurements and simulations of the absolute densities of $N_2(C)$ and $N_2^+(B)$. Model results are in qualitative agreement with measurements, underestimating the density of $N_2(C)$ by a maximum factor of eight.

Our study includes comparisons also for the absolute densities of other species [$N_2(B)$, $N(3p^4S)$ and $O(3p^5P)$], and the relative intensities of other radiative transitions [(SPS) $N_2(C,v)\rightarrow N_2(B,v')$; first negative system (FNS) $N_2^+(B,v=0)\rightarrow N_2^+(X,v'=0)$; atomic transitions $N(3p^4S)\rightarrow N(3s^4P)$ and $O(3p^5P)\rightarrow O(3s^5S)$], to be presented and discussed.

5. Final remarks

A low pressure, small radius microwave micro-plasma discharge has been analysed, using both simulations and measurements. For the particular conditions of this work, a transport theory for charged particles, including the effects of one negative ion species, has been successfully developed to simulate continuous wave micro-plasmas produced in capillary tubes. OES diagnostics were employed to measure the absolute densities of several species and the relative intensities of some radiative transitions. Simulation results evidence good qualitative agreement with measurements.

6. Acknowledgement

This work was partially supported by FCT - Fundação para a Ciência e a Tecnologia, under Project UID/FIS/50010/2013 and Project PLASMA-ADIST, and by the Labex LaSIPS, under Project MicroCap.

7. References

[1] U. Cvelbar, K. Ostrikov and M. Mozetic, "Reactive oxygen plasma-enabled synthesis of nanostructured CdO: tailoring nanostructures through plasma-surface interactions", *Nanotechnology* **19** (2008) 405605.

[2] D. Mariotti and R M. Sankaran, "Microplasmas for nanomaterials synthesis", *J. Phys. D: Appl. Phys.* **43** (2010) 323001.

[3] B. Debord, R. Jamier, F. Gérôme, O. Leroy, C. Boisse-Laporte, P. Leprince, L. L. Alves and F. Benabid, "Generation and confinement of microwave gas-plasma in photonic dielectric microstructure", *Opt. Express* **21** (2013) 25509.

[4] J. Mizeraczyk, M. Dors, M. Jasiński, B. Hrycak and D. Czylkowski, "Atmospheric pressure low-power microwave microplasma source for deactivation of microorganisms", *Eur. Phys. J. Appl. Phys.* **61** (2013) 24309.

[5] Y. Takao, K. Ono, K. Takahashi and K. Eriguchi, "Plasma diagnostics and thrust performance analysis of a microwave-excited microplasma thruster", *Jpn. J. Appl. Phys.* **45** (2006) 8235.

[6] V. Guerra and J. Loureiro, "Self-consistent electron and heavy-particle kinetics in a low pressure N_2-O_2 glow discharge", *Plasma Sources Sci. Technol.* **6** (1997) 373.

[7] V. Guerra and J. Loureiro, "Kinetic model of a low-pressure microwave discharge in O_2-N_2 including the effects of ions O^- on the characteristics for the plasma maintenance", *Plasma Sources Sci. Technol.* **8** (1999) 110.

[8] S. Dap, G. D. Stancu, O. Leroy, C. Boisse-Laporte, O. Leprince and T. Minea "Diagnostics of micro-plasmas generated by surface waves in capillary tubes, experiments and modelling of the plasma and the gas flow", *ICPIG 2013*, Granada, Spain.

[9] L. L. Alves, "The IST-LISBON database on LXCat", *J. Phys.: Conf. Ser.* **565** (2014) 012007; www.lxcat.net

[10] A. V. Phelps, "The diffusion of charged particles in collisional plasmas: free and ambipolar diffusion at low and moderate pressures", *J. Res. Natl. Inst. Stand. Technol.* **95** (1990) 407.

[11] S. A. Self and H. N. Ewald, "Static theory of a discharge column at intermediate pressures", *Phys. Fluids* **9** (1966) 2486.

[12] C. M. Ferreira and A. Ricard, "Modelling of the low-pressure argon positive column", *J. Appl. Phys.* **54** (1983) 2261.

[13] R. N. Franklin and J. Snell, "The free fall column with negative ions", *J. Phys. D: Appl. Phys.* **25** (1992) 453.

[14] C. M. Ferreira, G. Gousset and M. Touzeau, "Quasi-neutral theory of positive columns in electronegative gases", *J. Phys. D: Appl. Phys.* **21** (1988) 1403.

[15] Specair www.specair-radiation.net